Chinese Chemical Letters 36 (2025) 109845

Contents lists available at ScienceDirect

Chinese Chemical Letters

journal homepage: www.elsevier.com/locate/cclet

Ultrafast synthesis of Mo_2N with highly dispersed Ru for efficient alkaline hydrogen evolution

Xinyu Hou, Xuelian Yu*, Meng Liu, Hengxing Peng, Lijuan Wu, Libing Liao, Guocheng Lv*

Engineering Research Center of Ministry of Education for Geological Carbon Storage and Low Carbon Utilization of Resources, Beijing Key Laboratory of Materials Utilization of Nonmetallic Minerals and Solid Wastes, National Laboratory of Mineral Materials, School of Materials Science and Technology, China University of Geosciences (Beijing), Beijing 100083, China

ARTICLE INFO

Article history:
Received 3 March 2024
Revised 21 March 2024
Accepted 29 March 2024
Available online 30 March 2024

Keywords:
Mo_2N
Ruthenium
Electrocatalysis
Hydrogen evolution reaction
High temperature shock

ABSTRACT

Mo_2N has been identified as a highly promising carrier for electrocatalysis. However, its complex synthesis method, use of toxic gases, and serious effects on supported noble metals catalyst during high-temperature sintering processes have seriously affected its hydrogen evolution reaction (HER) activity and stability. Here, we report an efficient strategy for synthesizing Mo_2N using the high temperature shock (HTS) method in just 1.67 s, while also uniformly loading Ru onto Mo_2N nanosheets. The HTS enables the homogeneous dispersion of the noble metal Ru, leading to an increased electrocatalytic activity, along with a strong charge transfer between Mo_2N and Ru. Ru/Mo_2N exhibited an overpotential of 66 mV at 10 mA/cm^2 in 1 mol/L KOH. In the evaluation of catalytic activity, Ru/Mo_2N demonstrates superiority over commercial Pt/C catalysts in terms of mass activity (1.71 A/mgRu *vs.* 0.91 A/mgPt at 200 mV) and turnover frequency (1.41 s^{-1} *vs.* 0.18 s^{-1} at 100 mV). This result provides a rational and effective pathway for the preparation of efficient electrocatalysts.

H_2, with its high energy density (142,351 kJ/kg) and environmentally friendly nature, is considered the most promising alternative energy for resolving the environmental crisis [1,2]. Taking into account sustainable development, electrocatalytic water splitting has been recognized as a green and efficient method for H_2 production [3–6]. The alkaline hydrogen evolution reaction (HER) has gained recognition over the acidic HER due to its greater stability and cost-effectiveness, making it more suitable for large-scale applications [7].

Platinum (Pt) is well-known as one of the most effective noble metal catalysts for HER, primarily because of its moderate Pt-H bond [8,9]. However, Pt-based catalysts are expensive and impractical for large-scale applications. Recently, due to the excellent performance and significantly lower cost (approximately Pt∼4%), researchers considered ruthenium (Ru) as a promising electrocatalyst for HER [10]. While excessively strong OH adsorption by Ru monoatoms can lead to desorption difficulties and reduce the HER reaction rate [11]. Therefore, it is crucial to identify a suitable carrier with a strong water dissociation capacity to enhance the HER catalytic activity [12–14].

Transition metal nitrides (TMNs) are promising materials that can sustain HER activity at low noble metal loadings [15]. Studies have shown that the interaction between nitrogen (N) elements in TMNs with metals affects their electronic structures. The d orbitals of metal atoms will extend after being hybridized with the s and p orbitals of nitrogen atoms. This process gives them d-band characteristics similar to noble metals [16,17]. Compared to other carriers, such as transition metal carbides (TMCs), TMNs offer additional benefits by desorbing with extra nitrogen atoms as N_2 during synthesis, leaving a clean TMN surface for direct interaction with supported metal [18]. However, for TMCs, excess carbon may accumulate on the surface, preventing direct contact with the active metal [19]. In a recent study, Turaczy's team experimentally determined the hydrogen binding energy (HBE) value of molybdenum nitride, demonstrating its potential as a support to reduce noble metal loadings in HER catalysts [18]. The introduction of nitrogen atoms can alter the charge density of Mo atoms, effectively adjusting the strength of metal (Mo-H) bonds and optimizing electrochemical activity [20–22].

However, current synthesis methods of molybdenum nitrides under N_2 or NH_3 atmosphere typically involve high pressure and toxic gases (Table S1 in Supporting information) [23,24]. These methods often result in low yield and incomplete nitridation [25]. Besides, prolonged high-temperature reactions can lead to severe

* Corresponding authors.
E-mail addresses: xlyu@cugb.edu.cn (X. Yu), guochenglv@cugb.edu.cn (G. Lv).

https://doi.org/10.1016/j.cclet.2024.109845
1001-8417/

aggregation of Ru species [26,27]. Therefore, the rapid and safe synthesis of molybdenum nitride carriers with enhanced exposure and dispersion of Ru active sites remains a major challenge. High temperature shock (HTS) provides a simple and efficient strategy through rapid heating. Lattice defects generated by extremely rapid temperature changes can enhance the electronic polarization of elemental surfaces [28,29]. With this method, Hu's team successfully synthesized high-entropy alloys, which effectively addressed the aggregation of active sites and greatly simplified the synthesis path [30]. Similarly, niobium-based oxides have recently been synthesized through ultrafast carbon thermal shock (CTS) by Zhao *et al*., avoiding the need for time-consuming and energy-intensive annealing processes [31].

Based on the above considerations, we proposed an ultrafast (1.67 s) method to prepare Mo_2N and simultaneously evenly disperse ultrafine Ru sub-nanoparticles on the Mo_2N carrier. Under vacuum conditions, precursor powder was completely nitrided to Mo_2N by the rapid heating and cooling effects of HTS, and the interaction between Ru and Mo_2N effectively regulated the charge redistribution. The synthesized Ru/Mo_2N catalyst shows excellent HER performance under alkaline conditions (1 mol/L KOH). It exhibited a low overpotential of 66 mV *vs.* RHE for 10 mA/cm^2; it also maintains a significant advantage at an overpotential of 200 mV *vs*. RHE for 100 mA/cm^2, which is lower than commercial Pt/C (220 mV).

The specific synthesis method for Ru/Mo_2N is provided in the supporting information. In the synthesis of precursors, melamine and cyanuric acid have the ability to undergo self-association through hydrogen bonding in solution, while $Mo_7O_{24}^{6-}$ and Ru^{3+} can effectively anchor through the metal-N/O covalent bonding coordination effect [32,33]. After filtering and drying, the precursor powder was subjected to HTS for 1.67 s to form Ru/Mo_2N. In terms of structural characterization, we used X-ray diffraction (XRD) for compositional analysis of Ru/Mo_2N. In Fig. 1a, the diffraction peaks at 37.38°, 43.44°, 63.10°, and 75.95° are in good agreement with the characteristic crystal planes (111), (420), (311), and (200) of the cubic γ-Mo_2N (JCPDS card No. 25-1366). The significant bulge around 23° may be attributed to non-crystalline carbon. Meanwhile, Raman spectroscopy shows two distinct peaks of carbon: the D band (1342 cm^{-1}) and the G band (1586 cm^{-1}) (Fig. 1b). The value of I_D/I_G (1.16) further indicates the presence of non-crystalline carbon and numerous lattice defects in Ru/Mo_2N [34]. The morphology and structure of the prepared samples were investigated using scanning electron microscopy (SEM) and transmission electron microscopy (TEM). As shown in Fig. 1c, Ru/Mo_2N exhibits a curled nanosheet structure with open and continuous channels, and the specific surface area is 13.85 m^2/g. These channels may be derived from decomposable melamine and cyanuric acid, which are expected to enhance the accessibility of active sites [35,36]. Moreover, TEM images reveal a relatively high and uniform dispersion of Ru/Mo_2N (Fig. 1d). Notably, the carbon cladding layers were visualized in the TEM image (Fig. 1e), corresponding to the previously mentioned amorphous carbon. These carbon layers provide structural support to the entire Ru/Mo_2N particle and accelerate charge transfer. Furthermore, the lattice spacing of the Ru/Mo_2N sample was calculated to be 0.240 nm, corresponding to the (111) crystal plane of γ-Mo_2N. The structure of Ru/Mo_2N and the highly homogeneous dispersion of Mo, C, N, and Ru were further demonstrated by high-resolution TEM (HR-TEM) and energy-dispersive X-ray spectroscopy (EDS) mapping (Figs. 1f–j). Additionally, there are no obvious aggregates of Ru or its oxides on the entire nanosheet structure, indicating that Ru is dispersed as ultrafine sub-nanoparticles on the Mo_2N matrix [2].

In order to clarify the valence states of the chemical elements and their composition on the surface, X-ray photoelectron spectroscopy (XPS) was utilized. The XPS survey clearly shows signals of Mo, N, C, and Ru (Fig. 2a). The XPS spectra of Ru 3p (Fig. 2b) exhibits binding energies at 483.1 eV and 460.8 eV corresponding to the Ru $3p_{1/2}$ and Ru $3p_{3/2}$ peaks, respectively. Interestingly, the Ru 3p spectra of Ru/Mo_2N are negatively shifted compared to RuO_2 in other studies (486.3 eV and 464.1 eV), indicating an electron-enriched state in Ru species [37,38]. Fig. 2c shows N 1s XPS spectra in Ru/Mo_2N with two peaks located at 401.9 eV and 398.5 eV, corresponding to graphitic N and pyridinic N, respectively. The higher content of pyridinic N typically exhibits stronger alkalinity and nucleophilicity, making it capable of coordinating with metals. A typical N-Mo peak appears at 395.4 eV, indicating the presence of nitrides. The two peaks mentioned above collectively validate the existence of Mo_2N [39]. Fig. 2d displays the XPS spectrum of Mo 3d, showing three pairs of peaks corresponding to Mo^{2+}, Mo^{4+}, and Mo^{6+}. The peaks at 227.5 eV and 230.7 eV are attributed to Mo^{2+}, mainly derived from Mo_2N. The peaks at 228.3 eV and 233.1 eV correspond to Mo^{4+}, while the peaks at 231.8 eV and

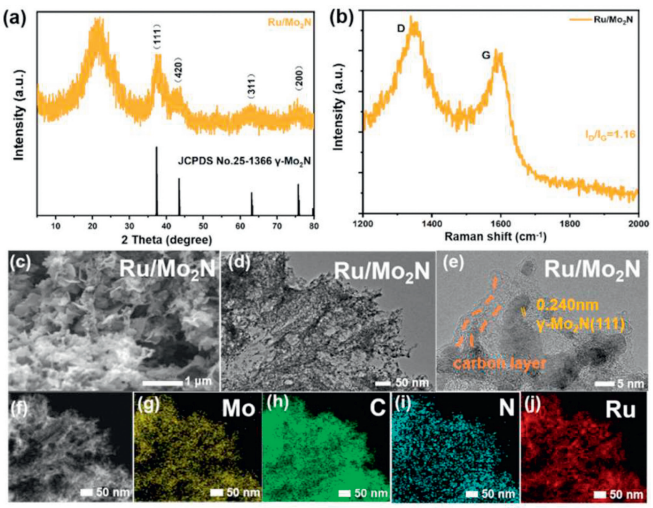

Fig. 1. Ru/Mo_2N: (a) XRD pattern. (b) Raman spectra. (c, d) SEM images. (e) TEM image. (f) HR-TEM image and (g-j) EDS mapping images.

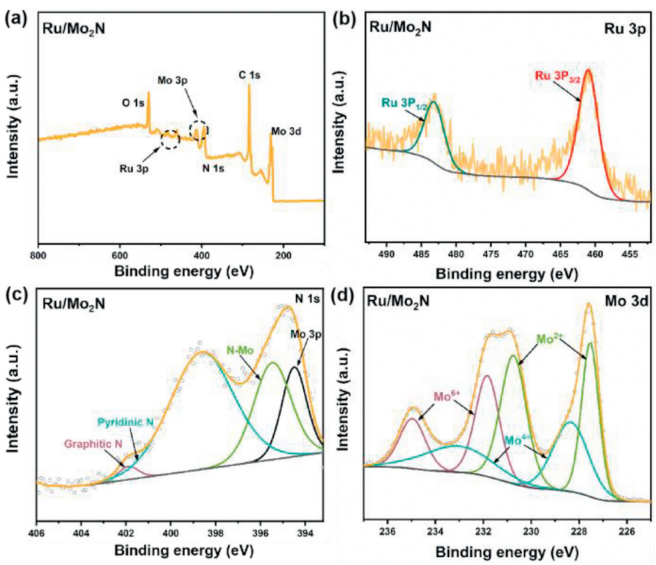

Fig. 2. The XPS spectra of Ru/Mo_2N. (a) XPS survey spectra of Ru/Mo_2N. (b) Ru 3p. (c) N 1s. (d) Mo 3d.

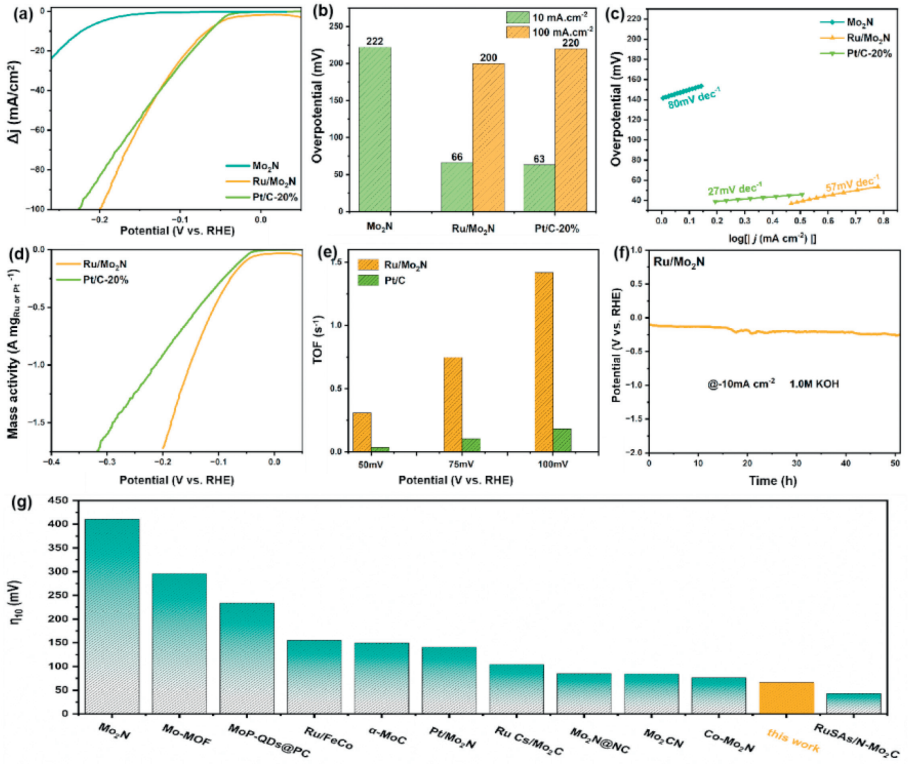

Fig. 3. (a–c) LSV curves, overpotentials and Tafel plots of Mo_2N, Ru/Mo_2N and Pt/C in 1 mol/L KOH. (d, e) Comparison of MA and TOF between Ru/Mo_2N and Pt/C. (f) Chronopotentiometric (CP) curve recorded at a constant current density of $-10\,mA/cm^2$. (g) The overpotential (η_{10}) of various Mo-N-based catalysts.

234.9 eV correspond to Mo^{6+}. The abundance of high-valence molybdenum attributes to the surface oxidation of Mo [40].

The electrochemical HER performance of Ru/Mo_2N was evaluated in 1 mol/L KOH electrolyte using a standard three-electrode system. All potentials are calculated with an iR correction and reported at a reversible hydrogen electrode (RHE) potential of $10\,mA/cm^2$. For comparison, the prepared samples and commercial Pt/C electrocatalysts were all tested. The preparation method for Mo_2N is similar to that of Ru/Mo_2N, except that Ru is not added. Linear sweep voltammetry (LSV) curves and overpotential in Figs. 3a and b show that the required overpotentials at $10\,mA/cm^2$ (η_{10}) and $100\,mA/cm^2$ (η_{100}) for Ru/Mo_2N are 66 mV and 200 mV, respectively, which are significantly lower than those of the contrast samples, Mo_2N ($\eta_{10} = 222$ mV) and commercial Pt/C ($\eta_{10} = 63$ mV, $\eta_{100} = 220$ mV). These results demonstrate that the inclusion of a trace amount of Ru significantly improved the electrocatalytic performance. We also studied the performance at different pH values (Fig. S1 in Supporting information). Moreover, the Tafel slope of Ru/Mo_2N in Fig. 3c is 57 mV/dec, which is lower than that of Mo_2N (80 mV/dec), suggesting faster kinetics on Ru/Mo_2N, believed to follow the Volmer-Heyrovsky mechanism [41,42]. In order to obtain a more precise study of Ru/Mo_2N, further calculations were performed on the mass activity (MA) and turnover frequency (TOF) related to the noble metals (Pt or Ru). MA represents the active species generated by the catalyst per unit mass, while TOF denotes the rate of reactant transformations per unit time in a catalyzed reaction. Impressively, the Ru/Mo_2N catalyst exhibits a significantly higher MA than commercial Pt/C (Fig. 3d), indicating a high utilization of noble metals. Additionally, it can be observed that at 50, 75, and 100 mV, the TOF of Ru/Mo_2N is also superior to Pt/C (Fig. 3e). Then, we assessed the electrocatalytic durability of the Ru/Mo_2N catalyst of η_{10} (Fig. 3f). After a 50-h prolonged test, the decay of the potential of the Ru/Mo_2N catalyst can be neglected, demonstrating its superior stability during the HER catalytic process. A range of previously reported Mo-N-based catalyst performances are demonstrated in Fig. 3g.

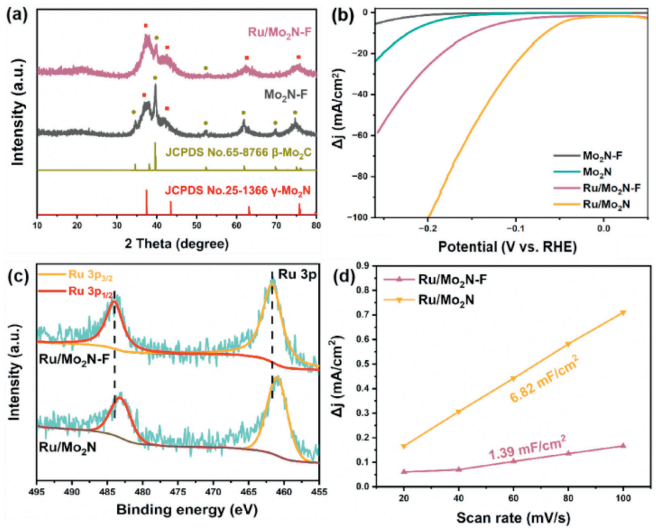

Fig. 4. (a) XRD patterns of Ru/Mo_2N and Ru/Mo_2N-F. (b) LSV curves of various samples in 1 mol/L KOH. (c) The XPS spectra of Ru 3p (Ru/Mo_2N and Ru/Mo_2N-F). (d) The electrochemical C_{dl} of Ru/Mo_2N and Ru/Mo_2N-F.

Furthermore, to validate the advantages of Mo_2N synthesized by HTS, Mo_2N-F and Ru/Mo_2N-F were prepared using the same raw materials but high-temperature tube furnace sintering method. Interestingly, the X-ray diffraction patterns of Mo_2N-F and Ru/Mo_2N-F (Fig. 4a), in addition to coinciding with some of the γ-Mo_2N peaks and also show good correspondence with the characteristic crystal planes (101), (110), (103), and (112) of hexagonal β-Mo_2C (JCPDS card No. 65–8766) at $2\theta = 39.58°$, 61.87°, 69.76°,

and 75.19°, respectively. Meanwhile, the crystal plane spacing of Ru/Mo_2N-F was calculated to be 0.228 nm and 0.236 nm based on the TEM images, corresponding to the (101) and (002) crystal faces of β-Mo_2C, respectively (Fig. S2 in Supporting information). The above results indicate that incomplete nitridation exists in Mo_2N-F and Ru/Mo_2N-F synthesized by high-temperature tube furnace sintering. EDS confirmed the uniform distribution of Mo, C, N, and Ru elements throughout the Ru/Mo_2N-F material (Figs. S3b-e in Supporting information). As for electrochemical HER performance, enormous distinctions were observed, LSV revealed that the overpotential (η_{10}) values of Mo_2N and Ru/Mo_2N (222 mV, 66 mV) were significantly lower than those of Mo_2N-F and Ru/Mo_2N-F (287 mV, 148 mV), as illustrated in Fig. 4b. To obtain a more precise investigation of these distinctions, XPS was employed (Fig. 4c). Compared with Ru/Mo_2N-F, the Ru 3p peak of Ru/Mo_2N shows a slight negative shift, implying a higher degree of electron transfer after HTS [43]. Meanwhile, the N 1s spectra of Ru/Mo_2N shows an obvious positive shift relative to that of Ru/Mo_2N-F (Fig. S4 in Supporting information). The above results suggest that there is an extensive interaction between Mo_2N and Ru species under HTS. To further compare the intrinsic HER activity of these samples, the electrochemical double-layer capacitance (C_{dl}) of the catalysts was determined by cyclic voltammetry (CV) as a function of scan rate (20–100 mV/s) (Fig. 4d) [44–46]. It is worth noting that the C_{dl} value of Ru/Mo_2N was 6.82 mF/cm^2, which was significantly higher than the C_{dl} value of Ru/Mo_2N-F (1.39 mF/cm^2). This also demonstrates that Ru/Mo_2N prepared by HTS disperses Ru more evenly, which possesses more catalytically active sites and exhibits higher catalytic activity.

In conclusion, we successfully developed a highly effective electrocatalyst, Ru/Mo_2N, using a rapid heating method, resulting in homogeneously dispersed Ru on Mo_2N. As evidenced by experimental analysis, we propose that the superior performance is attributed to a higher degree of electron transfer exhibited by Ru during the HTS, and a synergistic effect between highly dispersed Ru sub-nanoparticle sites and Mo_2N, promoting abundant metal-support interactions in Ru/Mo_2N. With an overpotential (η_{10}) of 66 mV and outstanding catalytic activity, the prepared Ru/Mo_2N catalyst exhibits its remarkable performance. The catalyst also demonstrates excellent long-term electrochemical stability in 1 mo/L KOH solution. This work provides a rational pathway for the preparation of Mo_2N-based electrocatalysts.

Declaration of competing interest

No conflict of interest exits in the submission of this manuscript, and manuscript is approved by all authors for publication. I would like to declare on behalf of my coauthors that the work described was original research that has not been published previously, and not under consideration for publication elsewhere, in whole or in part. All the authors listed have approved the manuscript that is enclosed.

CRediT authorship contribution statement

Xinyu Hou: Data curation, Methodology, Validation, Writing – original draft. **Xuelian Yu:** Supervision, Conceptualization, Formal analysis, Methodology. **Meng Liu:** Conceptualization, Data curation, Supervision, Validation. **Hengxing Peng:** Conceptualization. **Lijuan Wu:** Conceptualization, Software. **Libing Liao:** Methodology, Supervision. **Guocheng Lv:** Methodology, Resources, Supervision.

Acknowledgments

This work was supported by the Beijing Natural Science Foundation (No. 2232061) and the National Natural Science Foundation of China (No. 42377227).

Supplementary materials

Supplementary material associated with this article can be found, in the online version, at doi:10.1016/j.cclet.2024.109845.

References

[1] J.Q. Chi, M. Yallg, Y.M. Chai, et al., J. Energy Chem. 48 (2022) 398–423.
[2] X.L. Fan, C. Liu, M.Y. Wu, et al., Appl. Catal. B: Environ. 318 (2022) 121867.
[3] Y.M. Liu, Chem. Bio. Engin. 3 (2007) 79–81.
[4] B.H. Suryanto, Y. Wang, R.K. Hocking, et al., Nat. Commun. 10 (2019) 5599.
[5] S.D. Lu, B.Y. Lu, G.C. Tan, et al., Biosens. Bioelectron. 167 (2020) 112491.
[6] L.N. Chen, S.H. Wang, P.Y. Zhang, et al., Nano Energy 88 (2021) 106211.
[7] H.Q. Fu, M. Zhou, P.F. Liu, et al., J. Am. Chem. Soc. 144 (2022) 6028–6039.
[8] J.Y. Yu, A.Z. Wang, W.Q. Yu, et al., Appl. Catal. B: Environ. 277 (2020) 119236.
[9] D.Y. Ren, G.W. Wang, L.Y. Li, et al., Chem. Eng. J. 454 (2023) 140557.
[10] Y.N. Zhou, F.L. Wang, J. Nan, et al., Appl. Catal. B: Environ. 304 (2022) 120917.
[11] J. Zhang, G. Chen, Q. Liu, et al., Angew. Chem. Int. Ed. 61 (2022) e20220948.
[12] Z.X. Yang, Z.Z. Wang, J.T. Wan, et al., Environ. Sci. Technol. 56 (2022) 18008–18017.
[13] C. Li, H. Jang, M.G. Kim, et al., Appl. Catal. B: Environ. 307 (2022) 121204.
[14] H. Song, M. Wu, Z. Tang, et al., Angew. Chem. Int. Ed. 60 (2021) 7234–7244.
[15] X. Shi, A.P. Wu, H.J. Yan, et al., J. Mater. Chem. A 6 (2018) 20100–20109.
[16] C.G. Morales-Guio, L.A. Stern, X. Hu, Chem. Soc. Rev. 43 (2014) 6555–6569.
[17] X. Wang, J. He, B. Yu, et al., Appl. Catal. B: Environ. 258 (2019) 117996.
[18] K.K. Turaczy, W.J. Liao, et al., ACS Catal. 13 (2023) 14268–14276.
[19] Y.C. Kimmel, D.V. Esposito, R.W. Birkmire, et al., Int. J. Hydrogen Energy 37 (2012) 3019–3024.
[20] Y.Y. Chen, Y. Zhang, J. W, et al., ACS Nano 10 (2016) 8851–8860.
[21] D.J. Ham, J.S. Lee, Energies 2 (2009) 873–899.
[22] L. Zhe, M. Tahir, X.W. Lang, et al., J. Mater. Chem. A 5 (2017) 20932.
[23] K. Ojha, S. Saha, S. Banerjee, A.K. Ganguli, et al., ACS Appl. Mater. Interfaces 9 (2017) 19455–19461.
[24] L.M. Dai, F.L. Yao, L. Yu, et al., Adv. Energy Mater. 12 (2022) 2200974.
[25] J. Li, Y.N. Zhou, W.J. Tang, et al., Appl. Catal. B: Environ. 285 (2021) 119861.
[26] Z. Wei, P. Grange, B. Delmon, Appl. Surf. Sci. 135 (1998) 107–114.
[27] W.F. Chen, K. Sasaki, C. Ma, et al., Angew. Chem. Int. Ed. 51 (2012) 6131–6135.
[28] Z.X. Yang, Y. Li, X.T. Wang, et al., J. Environ. Sci. 142 (2024) 204–214.
[29] Z. Zhao, J. Sun, X. Li, et al., Appl. Catal. B 340 (2024) 123277–123293.
[30] Y. Yao, Z. Huang, P. Xie, et al., Science 359 (2018) 1489–1494.
[31] Q.L. Wu, Y.H. Kang, G.H. Chen, et al., Adv. Funct. Mater. (2024) 2315248.
[32] F. Chen, X.L. Wu, C. Shi, et al., Adv. Funct. Mater. 31 (2021) 2007877.
[33] B.X. Zhou, S.S. Ding, K.X. Yang, et al., Adv. Funct. Mater. 31 (2020) 2009230.
[34] J. Jia, T.L. Xiong, L.L. Zhao, et al., ACS Nano 11 (2017) 12509–12518.
[35] C. Tang, H. Zhang, K. Xu, et al., J. Mater. Chem. A 7 (2019) 18030–18038.
[36] L.N. Zhang, Z.L. Lang, Y.H. Wang, et al., Science 12 (2019) 2569–2580.
[37] P. Li, M. Wang, X.L. Duan, et al., Nat. Commun. 10 (2019) 1711.
[38] Y. Hu, G. Luo, L. Wang, et al., Adv. Energy Mater. 11 (2021) 2002816.
[39] A.C. Mtukula, X.J. Boand, L.P. Guo, J. Alloys Compd. 692 (2017) 614–621.
[40] Y.P. Zhu, G. Chen, X.M. Xu, et al., ACS Catal. 7 (2017) 3540–3547.
[41] M. Zeng, Y. Li, Mater. Chem. A 3 (2015) 14942–14962.
[42] M. Yao, H. Hu, B. Sun, et al., Small 15 (2019) 1905201.
[43] T.T. Chao, W.B. Xie, Y.M. Hu, et al., Energy Environ. Sci. 17 (2024) 1397–1406.
[44] J.S. Li, Y. Wang, C.H. Liu, et al., Nat. Commun. 7 (2016) 11204.
[45] K. Qu, Y. Zheng, X. Zhang, et al., ACS Nano 11 (2017) 7293–7300.
[46] C. Lu, D. Tranca, J. Zhang, et al., ACS Nano 11 (2017) 3933–3942.